This article has been accepted for publication in a future issue of this journal, but has not been fully edited. Content may change prior to final publication. Citation information: DOI 10.1109/TPEL.2016.2630711, IEEE Transactions on Power Electronics

An Electrolytic Capacitor-less Bi-directional EV Charger for V2G and V2H Applications

Minho Kwon, and Sewan Choi, *Senior Member, IEEE*

***Abstract*—In this paper, a bi-directional battery charger is proposed for grid-to-vehicle, vehicle-to-grid, and vehicle-to-home operations of electric vehicles. The proposed charger adopts sinusoidal charging to eliminate the use of electrolytic capacitors. A non-regulating series resonant converter is employed for isolation, thereby minimizing the ratings of the components and achieving zero-current switching turn ON and OFF of switches. Meanwhile, an ac–dc converter is employed to control each mode and their mode changes, making the whole control scheme simple and the mode changes seamless. A 3.3-kW prototype was built in the laboratory to validate the proposed concept. Our experimental results demonstrate that the proposed charger has high efficiency and can seamlessly switch between the three operation modes.**

***Index Terms* – bi-directional EV charger, on-board charger, vehicle-to-grid, vehicle-to-home, electrolytic capacitor-less, seamless**

I. INTRODUCTION

RECENTLY, electric vehicles (EVs) and plug-in hybrid electric vehicles (PHEVs) have been recognized as a promising transportation option to reduce fossil fuel usage and greenhouse emissions. The core devices in EVs consist of power conditioning units such as electric motors, inverters, dc–dc converters, and on-board battery chargers (OBCs). Among them, the OBC allows the traction battery in an EV to be charged using a standard outlet available at homes and offices. The basic functions of the OBC include battery charging, power factor correction (PFC), and galvanic isolation. The challenges for the OBC are power density, efficiency, reliability, and lifetime. Hence, power electronic technologies play an important role in improving the performance of EVs [1]–[4].

The basic operation of the OBC, called grid-to-vehicle (G2V), is to charge the traction battery. The battery can be utilized as an energy storage system with the help of vehicle-to-grid (V2G) technology [5]–[10] that allows stored energy to return to the grid according to a predefined schedule. Moreover, it can act as backup power for residential loads during a grid power outage by using vehicle-to-home (V2H) technology [9], [11]–[15]. Interest in the V2H function has greatly increased after the Fukushima disaster in Japan [13]. Obviously, the OBC should be bi-directional to implement not only the G2V but also the V2G and V2H technologies. Fig. 1 shows the three operating modes of the bi-directional EV charger, which are addressed in this paper.

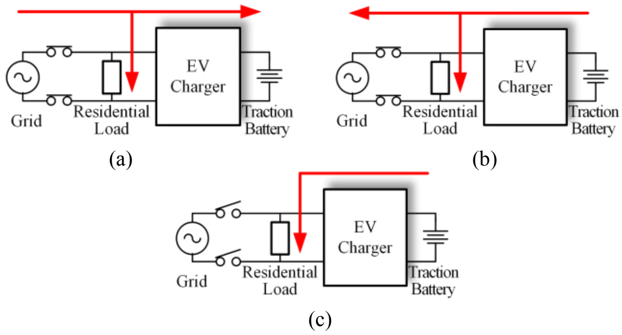

Fig. 1. Operating modes of the bi-directional EV charger. (a) G2V mode. (b) V2G mode. (c) V2H mode.

Typically, two-stage topologies, including an ac–dc converter and an isolated dc–dc converter, are considered for bi-directional EV chargers in [16]–[25]. A dual active bridge (DAB) converter is usually considered as an isolated dc–dc converter owing to its simple circuit structure and continuous power flow reversal capability [19]–[23]. However, it suffers from some drawbacks, such as limited zero-voltage switching range and high circulating current, under a wide voltage variation. Frequency-controlled resonant dc–dc converters were introduced for bi-directional operation in [26]–[28]. They can be expected to provide high efficiency and low electromagnetic interference emission owing to their soft-switching characteristics. However, they cannot continuously change the power flow because the switching patterns differ according to the direction of the power. A bidirectional LLC resonant converter was proposed in [29]. This topology can continuously switch between the forward and the backward modes, while maintaining the merits of conventional unidirectional LLC converter. However, most of resonant converters are quite sensitive to the tolerance of resonant components. It could be an impediment to mass production of the converter.

In general, the aforementioned two-stage topologies contain large dc-link electrolytic capacitors when they are used for constant-current/constant-voltage (CC/CV) charging to absorb two times the line frequency ripple (2LFR), which is a natural byproduct of single-phase ac–dc power conversion [30]. Electrolytic capacitors become an obstacle in achieving

This work was supported by the National Research Foundation of Korea grant funded by the Korea government (2014R1A2A2A01003724).

M. Kwon and S. Choi are with the Department of Electrical and Information Engineering, Seoul National University of Science and Technology, Seoul 01811, Korea (e-mail: saemnae@seoultech.ac.kr; schoi@seoultech.ac.kr).

This article has been accepted for publication in a future issue of this journal, but has not been fully edited. Content may change prior to final publication. Citation information: DOI 10.1109/TPEL.2016.2630711, IEEE Transactions on Power Electronics

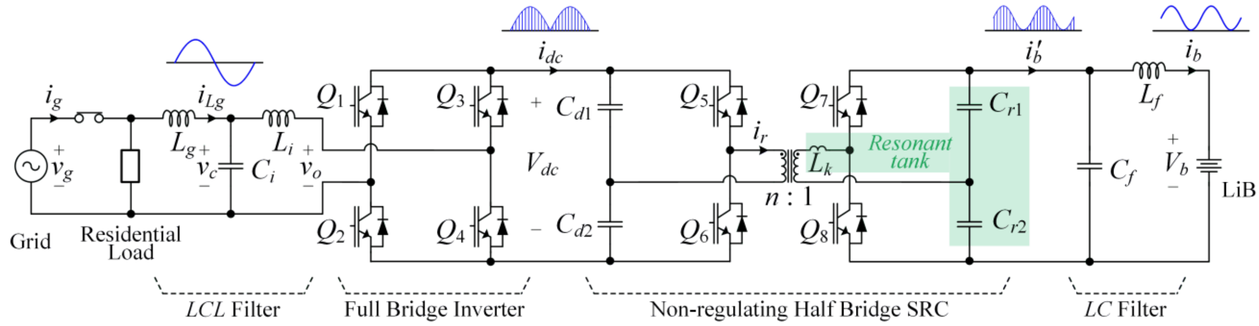

Fig. 2. Circuit diagram of the proposed bi-directional EV charger.

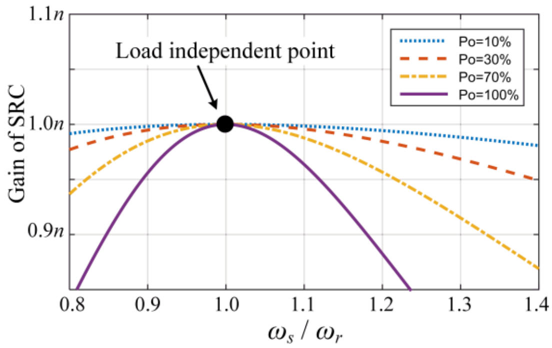

Fig. 3. Voltage-gain curve of SRC according to load variation.

high power density and long lifetime. In order to remove bulky electrolytic capacitors, an active power filter technique [31]-[34] can be considered. However, power loss, cost, and control complexity are increased, owing to the extra circuit.

In order to use small-value of film capacitors replace bulky electrolytic capacitors at dc-link, bi-directional EV chargers with sinusoidal charging were proposed in [22]–[23] and [25], where the chargers pass on 2LFR current to the battery. Previous reports state that 2LFR current to the battery causes a minor effect on the battery capacity and temperature rise [35]-[38].

A DAB-based electrolytic capacitors-less charger was proposed in [22]–[23], where the ac–dc converter is controlled to realize PFC and dc-link voltage regulation, and a DAB converter is used as an isolated dc–dc converter to control battery current. A control scheme that makes 2LFR current pass through the dc–dc converter as it flows to the battery is proposed to realize sinusoidal charging. In [25], a non-regulating LLC resonant converter-based charger was proposed for sinusoidal charging. This charger adopts an LLC resonant converter as an isolated ac-dc converter. Because this charger also employs small-value film capacitors at dc-link, the ac-dc converter generates the dc-link voltage of the rectified ac waveform which is converted to dc voltage with sinusoidal shaped battery current by the dc-dc converter. Use of a low bandwidth PI controller is required to regulate the average current of the battery, leading to slow dynamic performance. And this charger is not suitable for V2H operation because it cannot regulate the ac voltage for residential loads.

In the present paper, a bi-directional EV charger is proposed for the G2V, V2G, and V2H operations. The proposed charger adopts sinusoidal charging to eliminate the use of electrolytic capacitors. A non-regulating series resonant converter (SRC) is chosen as an isolated dc–dc converter of the proposed charger; thus, the SRC achieves zero-current switching (ZCS) turn ON and OFF under an entire load range in the sinusoidal charging method, where the charging current pulsates at 2LFR, resulting in high efficiency. Whereas the SRC operates like a dc transformer, the ac–dc converter is controlled to perform not only PFC but also G2V, V2G, or V2H operation, which simplifies the control scheme for each mode and mode change. In this paper, issues associated with mode change are discussed, and seamless mode change between the three operations is realized.

II. Proposed Bi-directional Charger

A. Circuit Configuration

Fig. 2 shows the circuit diagram of the proposed bi-directional EV charger. The proposed charger consists of two power conversion stages: a single-phase full-bridge inverter with an *LCL* filter and a non-regulating half-bridge SRC with an *LC* filter. Capacitors C_{d1} and C_{d2} are designed to absorb only high-frequency (HF) switching ripples generated from both the inverter and SRC. Thus, low-frequency components are delivered through the SRC to the battery side. The *LC* filter on the battery side is designed to prevent HF ripples generated by the SRC from flowing into the battery, whereas the low-frequency components are allowed to flow through the battery for sinusoidal charging. We note that all capacitors of the proposed charger are used for filtering the HF components, thereby allowing the use of film capacitors.

B. Operation Analysis

Resonant capacitors C_{r1} and C_{r2} generate resonance with transformer leakage inductance L_k, as shown Fig. 2. The resonant frequency of the SRC is determined as follows:

$$\omega_r = \frac{1}{\sqrt{L_k (C_{r1} + C_{r2})}}. \tag{1}$$

On the basis of the fundamental harmonic approximation [39], the voltage gain of the SRC can be expressed as follows:

$$G_{SRC} = n \cdot \frac{1}{1 + j\dfrac{\pi^2}{8} \cdot Q\left(\dfrac{\omega_s}{\omega_r} - \dfrac{\omega_r}{\omega_s}\right)} \tag{2}$$

where n is the turn ratio of the transformer. ω_s and Q are the

This article has been accepted for publication in a future issue of this journal, but has not been fully edited. Content may change prior to final publication. Citation information: DOI 10.1109/TPEL.2016.2630711, IEEE Transactions on Power Electronics

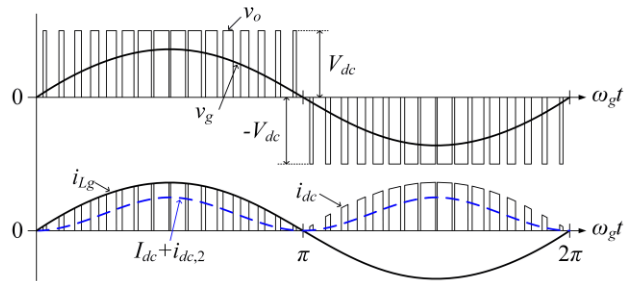

Fig. 4. Key waveforms of the inverter with unipolar voltage switching.

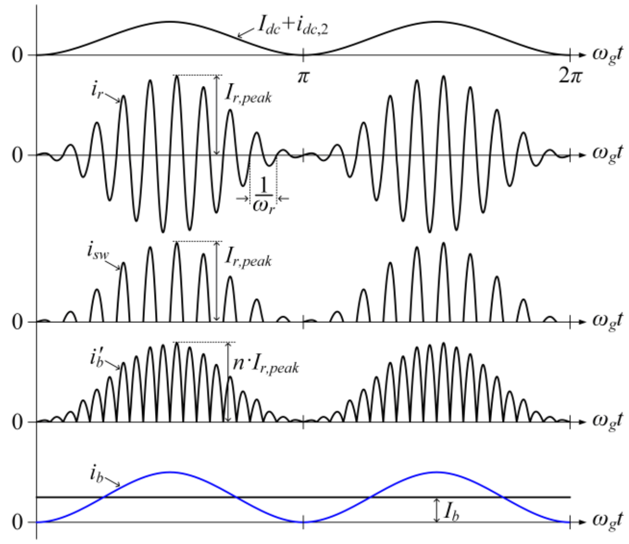

Fig. 5. Key current waveforms of the SRC containing second harmonic.

switching frequency and quality factor of the SRC, respectively. Fig. 3 shows the voltage-gain curves according to the load variation. When ω_s is equal to ω_r, the voltage gain of the SRC is constant even though the load condition changes. This point is called the load-independent point. Moreover, the operation at this point makes all switches of the SRC achieve both ZCS turn ON and OFF irrespective of the load variation. The SRC operates with half duty cycle and fixed switching frequency at the load-independent point. The voltage-gain curves are designed to be flat by using a small value for L_k, which leads to little effect on the tolerance of the resonant components [40], [41]. Therefore, from (2), the voltage gain of the SRC can be simplified as follows:

$$G_{SRC} \approx n\,. \tag{3}$$

Resonant current i_r depends on input current i_{dc} as follows [39]:

$$i_r(t) = \pi i_{dc}(t)\sin(\omega_r t)\,. \tag{4}$$

To avoid resonance with L_k, C_{d1} and C_{d2} and filter capacitor C_f should be sufficiently larger than C_{r1} and C_{r2}. In this work, C_f is selected to be 50 times the resonant capacitance as follows:

$$C_f = 50(C_{r1}+C_{r2})\,. \tag{5}$$

In the same manner, C_{d1} and C_{d2} are chosen to be

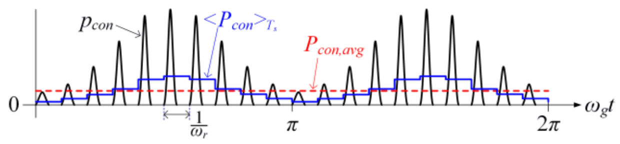

Fig. 6. Waveforms of conduction loss in one switch.

$$C_{d1} = C_{d2} = 50\left(\frac{C_{r1}+C_{r2}}{n^2}\right). \tag{6}$$

Then, filter inductor L_f can be determined as follows:

$$L_f = \frac{1}{\omega_c^2 C_f} \tag{7}$$

where ω_c is the cutoff frequency at the battery-side LC filter. To damp the resonant frequency component, as a rule of thumb, the cutoff frequency is selected to be smaller than 1/10 of ω_r.

Fig. 4 shows the key waveforms of the inverter with unipolar voltage switching. Assuming that the switching frequency of the inverter approaches infinity and therefore the energy stored in the LCL filter is negligible, the instantaneous power input must equal the instantaneous power output of the LCL filter. Then, the dc-side current of the inverter can be expressed as follows:

$$i_{dc}(t) = \frac{v_o(t)i_{Lg}(t)}{V_{dc}}\,. \tag{8}$$

We let grid voltage v_g and grid-side inductor current i_{Lg} be pure sine waves at fundamental angular frequency ω_g as follows:

$$v_{o,1}(t) = v_g(t) = \sqrt{2}V_g \sin\omega_g t \tag{9}$$

$$i_{Lg}(t) = \sqrt{2}I_{Lg}\sin(\omega_g t - \phi) \tag{10}$$

where $v_{o,1}$ is the fundamental component of v_o and ϕ is the angle by which i_{Lg} lags v_g. Then, the dc-side current of the inverter can be rewritten as follows:

$$i_{dc}(t) = \frac{V_g I_{Lg}}{V_{dc}}\cos\phi - \frac{V_g I_{Lg}}{V_{dc}}\cos(2\omega_g t-\phi) + HF\ term\,. \tag{11}$$

When the power factor is unity, the dc and second-harmonic components of i_{dc} can be respectively obtained as follows:

$$I_{dc} = \frac{V_g I_{Lg}}{V_{dc}}\,. \tag{12}$$

$$i_{dc,2}(t) = -I_{dc}\cos 2\omega_g t\,. \tag{13}$$

Because the HF term generated on the dc side of the inverter is absorbed by C_{d1} and C_{d2}, only the dc and second-harmonic components are transferred to the SRC.

Fig. 5 shows the key waveforms of the SRC. From (4), (12), and (13), the resonant current containing second-harmonic can be obtained by

$$i_r(t) = \pi I_{dc}(1-\cos 2\omega_g t)\sin\omega_r t\,. \tag{14}$$

This article has been accepted for publication in a future issue of this journal, but has not been fully edited. Content may change prior to final publication. Citation information: DOI 10.1109/TPEL.2016.2630711, IEEE Transactions on Power Electronics

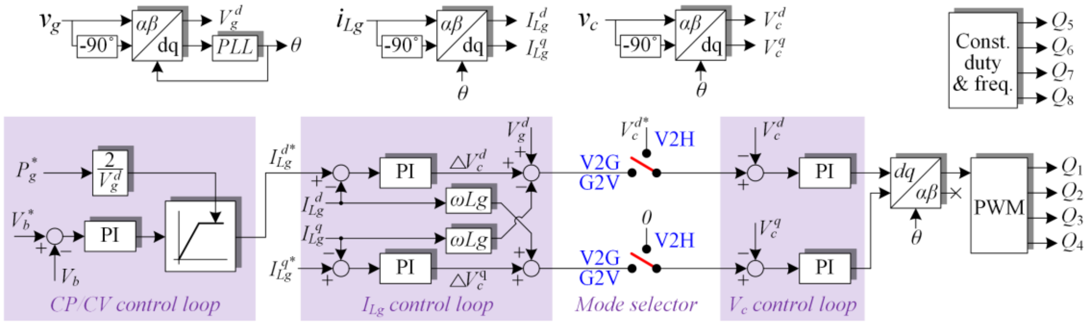

Fig. 7. Proposed control block diagram for G2V, V2G, and V2H operations.

Assuming $\omega_r >> \omega_g$, the RMS value of i_r can be obtained using (14) by

$$I_{r,RMS} = \sqrt{\frac{1}{2\pi}\int_0^{2\pi} i_r^2 d\omega_g t} = \sqrt{3}\cdot\frac{\pi}{2}I_{dc}. \tag{15}$$

From (14), the peak value of i_r becomes

$$I_{r,peak} = 2\pi I_{dc} \tag{16}$$

which is the same as the peak current of dc-side switches Q_5 and Q_6. Using (15), the RMS current of switches Q_5 and Q_6 can be obtained by

$$I_{sw,RMS} = \frac{I_{r,RMS}}{\sqrt{2}} = \sqrt{\frac{3}{2}}\cdot\frac{\pi}{2}I_{dc}. \tag{17}$$

The current ratings of battery-side switches Q_7 and Q_8 are the same as n times those of switches Q_5 and Q_6.

The LC filter is designed to filter the resonant frequency component from the output current of the SRC such that the battery current has dc and second-harmonic components as follows:

$$i_b(t) = I_b(1-\cos 2\omega_g t) \tag{18}$$

where $I_b = V_g I_{Lg} / V_b$.

C. Conduction Loss Analysis

Power dissipation in a switch during conduction can be expressed as follows:

$$p_{con}(t) = v_{on}(t) i_{sw}(t) \tag{19}$$

where v_{on} and i_{sw} are the on-state voltage and current, respectively. The on-state voltage of an IGBT can be obtained as follows:

$$v_{on}(t) = V_{CE0} + R_{on} i_{sw}(t) \tag{20}$$

where V_{CE0} is the collector-emitter saturation voltage and R_{on} is the on-state resistance. During conduction, the on-state current of a dc-link side switch of the SRC is equal to $i_r(t)$. Thus, the instantaneous power dissipation in the switch can be rewritten using equation (14) and (19)-(20) as follows:

$$\begin{aligned} p_{con}(t) &= V_{CE0}\pi I_{dc}(1-\cos 2\omega_g t)\sin\omega_r t \\ &\quad + R_{on}\pi^2 I_{dc}^2 (1-\cos 2\omega_g t)^2 \sin^2 \omega_r t \end{aligned}. \tag{21}$$

Because $\omega_r >> \omega_g$, $p_{con}(t)$ can be expressed as a function of $\theta_r(=\omega_r t)$ as follows:

$$\begin{aligned} p_{con}(\theta_r) &= V_{CE0}\pi I_{dc}(1-\cos 2\theta_g)\sin\theta_r \\ &\quad + R_{on}\pi^2 I_{dc}^2 (1-\cos 2\theta_g)^2 \sin^2\theta_r \end{aligned} \tag{22}$$

where θ_g $(=\omega_g t)$ is considered to be constant during the switching period. Then, instantaneous average conduction loss in one switching period can be calculated as follows:

$$\begin{aligned} < P_{con} >_{T_s} &= \frac{1}{2\pi}\int_0^{\pi} p_{con}(\theta_r)d\theta_r \\ &= V_{CE0}I_{dc}(1-\cos 2\theta_g) + \frac{\pi^2}{4}R_{on}I_{dc}^2(1-\cos 2\theta_g)^2 \end{aligned} \tag{23}$$

where $T_s = 2\pi/\omega_r$. Consequently, the average conduction loss of the switch is determined as follows:

$$\begin{aligned} P_{con,avg} &= \frac{1}{\pi}\int_0^{\pi} < P_{con} >_{T_s} d\theta_g \\ &= V_{CE0}I_{dc} + \frac{3}{8}\pi^2 R_{on} I_{dc}^2 \end{aligned}. \tag{24}$$

Fig. 6 shows waveforms of the instantaneous power dissipation, the instantaneous average conduction loss and the average conduction loss in a switch of the SRC. Switching losses of the SRC are negligible owing to ZCS operation. Major sources of power dissipation in the proposed charger include the SRC conduction loss, HF transformer loss, ac-dc stage conduction, and switching losses.

D. Control Strategy

Fig. 7 shows the control block diagram for the G2V, V2G, and V2H operations of the proposed bi-directional EV charger. It consists of three control loops: an outer *CP/CV control loop*, a middle I_{Lg} *control loop*, and an inner V_c *control loop*. When the grid voltage is normal, the charger is connected to the grid and can be operated in either G2V or V2G mode. Battery voltage reference V_b^* is usually set as the full-charge voltage of the battery. When the battery is not fully charged, the output of the proportional–integral (PI) compensator in the *CP/CV control loop* is saturated by the limiter, and grid-side current reference I_{Lg}^{d*} is determined by the upper limit value of the limiter as follows:

$$I_{Lg}^{d*} = \frac{2}{V_g^d}P_g^*. \tag{25}$$

This article has been accepted for publication in a future issue of this journal, but has not been fully edited. Content may change prior to final publication. Citation information: DOI 10.1109/TPEL.2016.2630711, IEEE Transactions on Power Electronics

TABLE I
CONTROL TARGET COMPARISON OF THE CONVENTIONAL AND THE PROPOSED METHODS

Operating mode	Conventional method I [14]		Conventional method II [15]		Proposed method	
	inverter	dc–dc converter	inverter	dc–dc converter	inverter	dc–dc converter
G2V	*dc-link voltage*	*CC/CV*	*dc-link voltage*	*CC/CV*	*CP/CV*	*no regulation*
V2G	*CP*	*dc-link voltage*	*CP*	*CP*	*CP*	*no regulation*
V2H	*ac voltage*	*dc-link voltage*	*ac voltage*	*dc-link voltage*	*ac voltage*	*no regulation*

TABLE II
COMPARISON OF BIDIRECTIONAL CHARGERS

Topology	[19], [20]	[22], [23]	[25]	Proposed charger
	DAB based	DAB based	Non-regulating LLC based	Non-regulating SRC based
Optimized design of isolation stage	No	No	Yes	Yes
DC-link capacitor	Electrolytic	Film	Film	Film
Charging method	DC	Sinusoidal	Sinusoidal	Sinusoidal
Operating modes	G2V, V2G	G2V, V2G	G2V, V2G	G2V, V2G, V2H
Control bandwidth	Wide	Wide	Narrow	Wide
Switching characteristic of isolation stage	Conditional ZVS turn ON & hard switching turn OFF	Conditional ZVS turn ON & hard switching turn OFF	ZVS turn ON & small turn OFF current	ZCS turn ON & OFF

where P_g^* is the desired amount of power for either charging (G2V) or discharging (V2G). An anti-windup mechanism must be implemented in the PI compensator to limit the integrator. When V_b reaches the full-charge voltage, the PI compensator in the *CP/CV control loop* is activated to regulate the battery voltage. The outputs of the *I_{Lg} control loop* become the references of the *V_c control loop*. We note that i_{Lg} is indirectly controlled by the magnitude and phase of v_c with respect to v_g [42]. When the grid voltage fails, the charger is disconnected from the grid, and the references of the *V_c control loop* are changed into the V2H mode by the *Mode selector*; thus, the ac-side voltage for residential loads can be regulated by the *V_c control loop*.

III. COMPARATIVE STUDIES

The control targets of the proposed and conventional methods [14], [15] that deal with V2G and V2H are listed in Table I. The control targets are altered along with the operating modes, which may cause transient issues during the mode change. Fig. 8 shows the mode-transition performance of the conventional methods and the proposed method. In the conventional methods, both the inverter and the dc–dc converter take part in the control and mode change, whereas in the proposed method, the dc–dc converter is not regulated, and the inverter only plays a role in the control and mode change. Therefore, the proposed method can achieve smooth transition, which is mainly due to the common inner *V_c control loop* [42]. Thus far, a bidirectional charger that can manage V2H operation with seamless mode changes has not been presented.

Table II shows the characteristics of the proposed charger in comparison with conventional chargers [19]-[20], [22]-[23] and [25]. The non-regulating isolation stage, which operate at the load-independent point, contributes to the optimal designs of the transformer, resonant components, and switching devices. When a resonant converter is operated at the load-independent point, a switch can achieve ZVS turn ON using magnetizing current as in [25]. However, this may increase circulating current and turn off current. The proposed SRC is operated at load-independent point with minimized magnetizing current, thereby achieving ZCS turn ON, which leads to negligible circulating current and ZCS turn OFF. A turn on loss associated with the discharge energy of the output capacitor of a switch can be minimized by selecting a switch with small output capacitance and adjusting the dead-time between switches in the same leg [41].

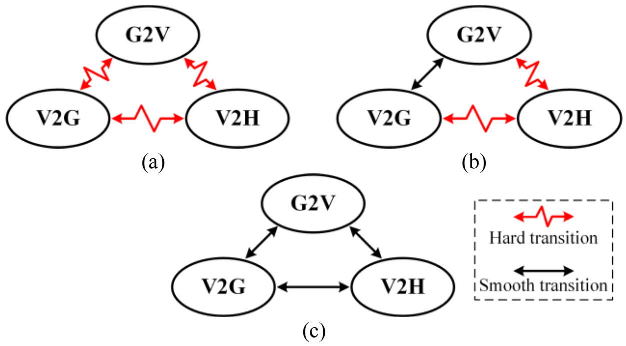

Fig. 8. Diagram showing the mode-transition performance. (a) Conventional method I [14]. (b) Conventional method II [15]. (c) Proposed method.

IV. EXPERIMENTAL RESULTS

Experimental results from a 3.3-kW prototype, which is shown in Fig. 9, are provided to validate the performance of the proposed bi-directional EV charger. The prototype was

This article has been accepted for publication in a future issue of this journal, but has not been fully edited. Content may change prior to final publication. Citation information: DOI 10.1109/TPEL.2016.2630711, IEEE Transactions on Power Electronics

TABLE III
PARAMETERS OF THE PROTOTYPE

Parameters	Symbols	Values
Grid-side filter inductance	L_i	2 × 1.2 [mH]
	L_g	1.7 [mH]
Grid-side filter capacitance	C_i	6.8 [µF]
Battery-side filter inductance	L_f	33 [µH]
Battery-side filter capacitance	C_f	100 [µF]
Resonant capacitance	C_{r1}, C_{r2}	1 [µF]
Leakage (resonant) inductance	L_k	4.7 [µF]
dc-link capacitance	C_{d1}, C_{d2}	100 [µF]
Transformer turn ratio	n	1.4

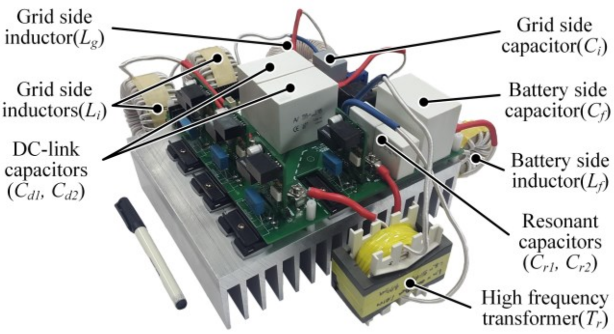

Fig. 9. Photograph of a 3.3-kW prototype of the proposed EV charger.

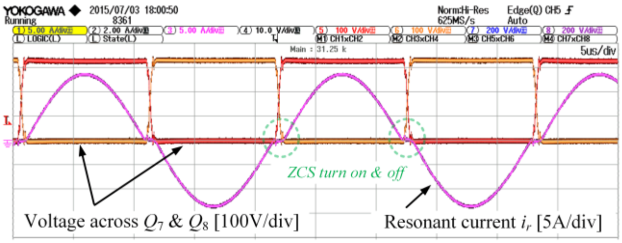

Fig. 10. Experimental waveforms showing ZCS operation of the battery-side switches of the proposed SRC.

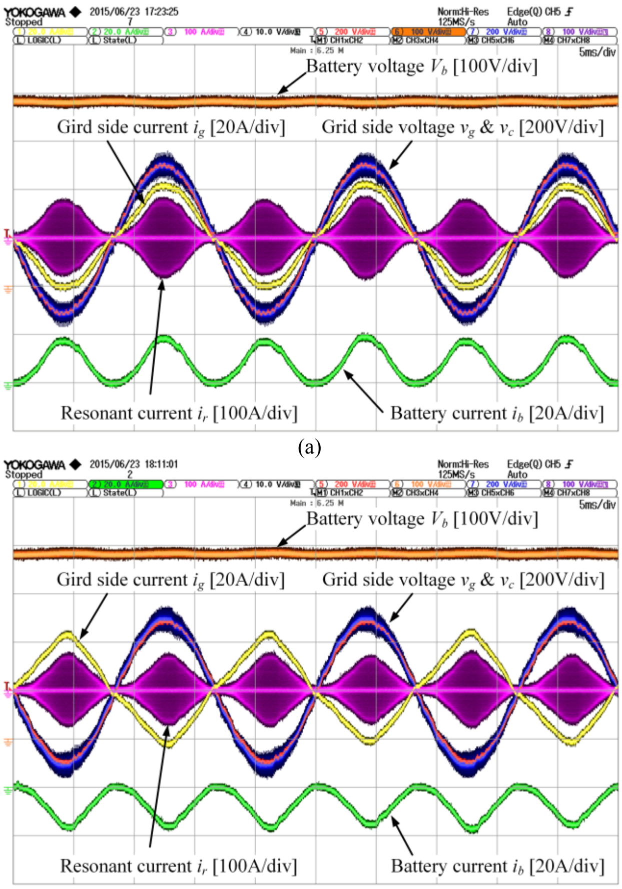

Fig. 11. Experimental waveforms showing the grid-connected operation of the proposed charger. (a) G2V mode. (b) V2G mode.

built according to the following specifications: P_o = 3.3 kW, V_g = 220 V, f_g = 60 Hz, and V_b = 250 to 410 V. The parameters of the prototype are listed in Table III. All switches were implemented using high-speed switching IGBTs (IKW50N65H5 from Infineon). The HF transformer was implemented with a ferrite core (PQ78/39 from TDK). *LCL* filter inductors L_g and L_i were implemented with powder cores (CH610125 from Changsung), and *LC* filter inductor L_f was implemented with a powder core (CH467125 from Changsung). The control algorithm was implemented by a digital signal processor (TMS320F28335 from TI).

Fig. 10 shows that the battery-side switches of the SRC are turned ON and OFF under ZCS condition. Note that because the output capacitance of the implemented switches is very small, voltage across the switch is quickly discharged at the turn off instant although discharging current is nearly zero, where 500ns of dead-time was implemented. In the same manner, the inverter-side switches of the SRC are also operated under ZCS condition. Fig. 11 shows the grid-connected operation of the proposed charger. Both battery current i_b and resonant current i_r contain 2LFR. The battery is charged and discharged with sinusoidal-like current, as shown in Figs. 11 (a) and (b), respectively. Fig. 12 shows the experimental waveforms of the mode change from G2V to V2H and from V2G to V2H. The experimental results show little transient in spite of the occurrence of an unexpected grid power outage.

The measured efficiencies in the G2V and V2G modes according to the battery voltage are shown in Fig. 13. The efficiencies were measured using Yokogawa WT3000. The peak efficiencies in the charging and discharging modes occur at 600 W and are 95.7% and 95.4%, respectively.

Fig. 14 shows the loss distribution of the proposed charger in different powers and battery voltages. When the battery voltage is high, switching loss in the ac-dc stage is increased owing to a higher switching voltage that is proportional to the battery voltage; and the core loss of the HF transformer is also increased, owing to increased volt-seconds across the transformer. However, a large portion of the power dissipation in the proposed charger appears as conduction loss, owing to negligible switching loss in the SRC, especially in heavy load condition. Hence, as the battery voltage increases, the drop in the efficiency curve according to the output power tends to be small, as shown in Fig. 13.

V. CONCLUSIONS

In this paper, an electrolytic capacitor-less bi-directional EV charger has been proposed to realize V2G and V2H func-

This article has been accepted for publication in a future issue of this journal, but has not been fully edited. Content may change prior to final publication. Citation information: DOI 10.1109/TPEL.2016.2630711, IEEE Transactions on Power Electronics

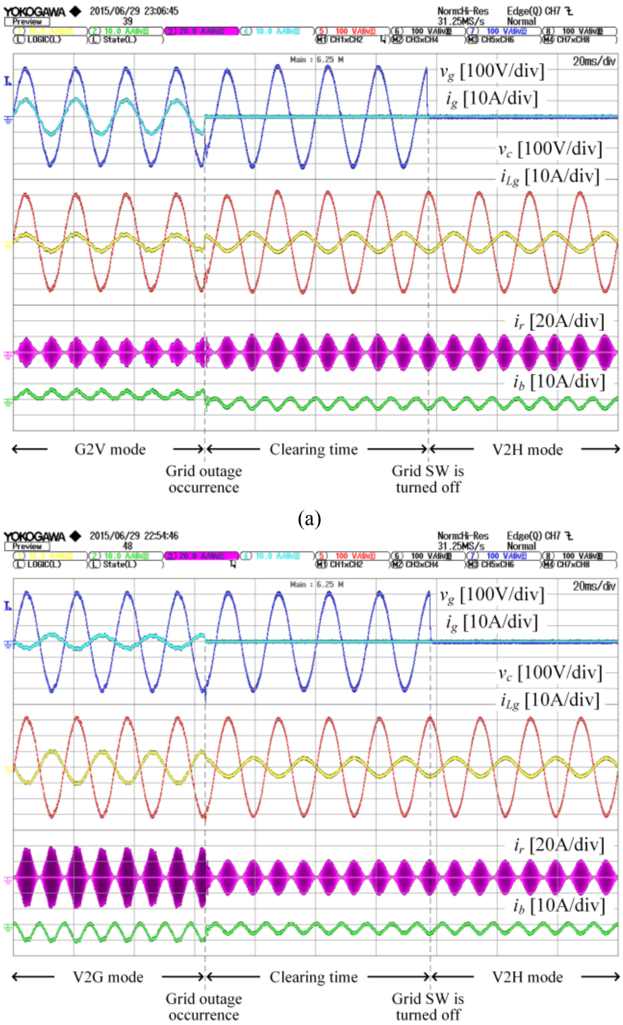

Fig. 12. Experimental waveforms of the proposed EV charger showing the mode change. (a) G2V to V2H. (b) V2G to V2H.

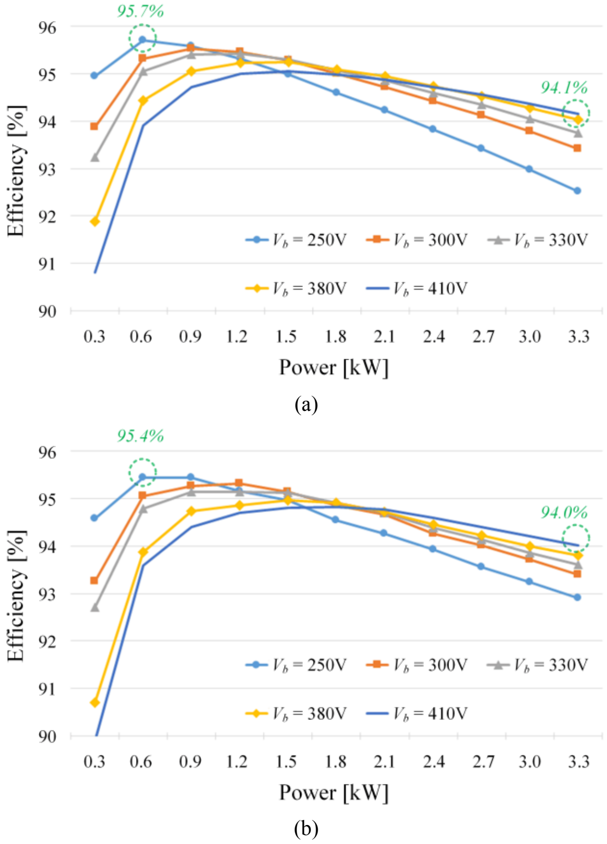

Fig. 13. Measured efficiency according to the battery voltage. (a) Charging mode. (b) Discharging mode.

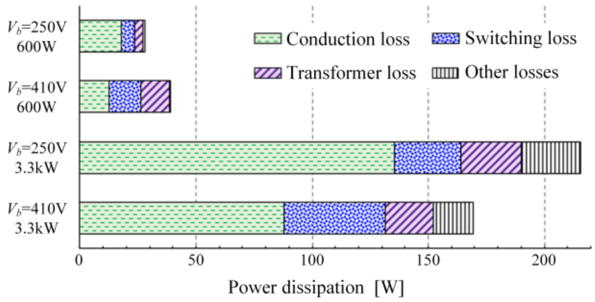

Fig. 14. Loss distribution of the proposed chrager according to the battery voltage and output power.

tions. By applying the sinusoidal charging method to the proposed EV charger, the proposed charger eliminates the need for an electrolytic capacitor. The SRC achieves ZCS turn ON and OFF under an entire load condition. The common inner loop of the proposed control block is demonstrated to provide seamless mode change between each mode of operation. Experimental results from a 3.3-kW prototype are provided to validate the proposed control method. The measured efficiency curves show that both charging and discharging operations are almost identical. The peak measured efficiencies of the proposed charger at 600 W are 95.7% in the charging mode and 95.4% in the discharging mode.

REFERENCES

[1] Emadi, S. S. Williamson, and A. Khaligh, "Power electronics intensive solutions for advanced electric, hybrid electric, and fuel cell vehicular power systems," *IEEE Trans. Power Electron.*, vol. 21, no. 3, pp. 567–577, May. 2006.

[2] Emadi, Y. Lee, and K. Rajashekara, "Power electronics and motor drives in electric, hybrid electric, and plug-in hybrid electric vehicles," *IEEE Trans. Ind. Electron.*, vol. 55, no. 6, pp. 2237–2245, Jun. 2008.

[3] L. Dickerman and J. Harrison, "A new car, a new grid," *IEEE Power Energy Mag.*, vol. 8, no. 2, pp. 55–61, Mar./Apr. 2010.

[4] C. C. Chan, "The state of the art of electric, hybrid, and fuel cell vehicles," *Proc. IEEE*, vol. 95, no. 4, pp. 704–718, Apr. 2007.

[5] S. Han, S. Han, and K. Sezaki, "Development of an optimal vehicle-to-grid aggregator for frequency regulation," *IEEE Trans. Smart Grid*, vol. 1, no. 1, pp. 65–72, Jun. 2010.

[6] E. Sortomme, and M. A. El-Sharkawi, "Optimal charging strategies for unidirectional vehicle-to-grid," *IEEE Trans. Smart Grid*, vol. 2, no. 1, pp. 131–138, Mar. 2011.

[7] W. Su, H. Rahimi-Eichi, W. Zeng, and M. Chow, "Survey on the Electrification of Transportation in a Smart Grid Environment," *IEEE Trans. Ind. Inform.*, vol. 8, no. 1, pp. 1–10, Feb. 2012.

[8] M. Yilmaz, and P. T. Krein, "Review of the impact of vehicle-to-grid technologies on distribution systems and utility interfaces," *IEEE Trans. Power Electron.*, vol. 28, no. 12, pp. 5673–5689, Dec. 2013.

[9] C. Liu, K. T. Chau, D. Wu, and S. Gao, "Opportunities and challenges of vehicle-to-home, vehicle-to-vehicle, and vehicle-to-grid technologies," *Proc. IEEE*, vol. 101, no. 11, pp. 2409–2427, 2013.

[10] M. C. Kisacikoglu, M. Kesler, and L. M. Tolbert, "Single-phase on-board bidirectional PEV charger for V2G reactive power operation," *IEEE Trans. Smart Grid*, vol. 6, no. 2, pp. 767–775, Mar. 2015.

[11] O. Erdinc, N. G. Paterakis, T. D. P. Mendes, A. G. Bakirtzis, and J. P. S. Catalão, "Smart household operation considering bi-directional

This article has been accepted for publication in a future issue of this journal, but has not been fully edited. Content may change prior to final publication. Citation information: DOI 10.1109/TPEL.2016.2630711, IEEE Transactions on Power Electronics

EV and ESS utilization by real-time pricing-based DR," *IEEE Trans. Smart Grid*, vol. 6, no. 3, pp. 1281–1291, May. 2015.

[12] N. Z. Xu, and C. Y. Chung, "Reliability evaluation of distribution systems including vehicle-to-home and vehicle-to-grid," *IEEE Trans. Power Systems*, vol. 31, no. 1, pp. 759–768, Jan. 2016.

[13] D. P. Tuttle, R. L. Fares, R. Baldick, and M. E.Webber, "Plug-in vehicle to home (V2H) duration and power output capability," in *Proc. IEEE Transp. Electrif. Conf. Expo, Compon., Syst. Power Electron., Technol. Bus. Public Policy*, Dearborn, MI, USA, Jun. 16–19, 2013, pp. 1–7.

[14] X. Zhou, G. Wang, S. Lukic, S. Bhattacharya, and A. Huang, "Multi-function bi-directional battery charger for plug-in hybrid electric vehicle application," in *Proc. IEEE Energy Conversion Congr. Expo.*, Sep. 2009, pp. 3930–3936.

[15] J. G. Pinto, V. Monteiro, H. Goncalves, B. Exposto, D. Pedrosa, C. Couto, J. L. Afonso, "Bidirectional battery charger with grid-to-vehicle, vehicle-to-grid and vehicle-to-home technologies," in *Proc. IECON*, 2013, pp. 10–13.

[16] M. Yilmaz, and P. T. Krein, "Review of battery charger topologies, charging power levels, and infrastructure for plug-in electric and hybrid vehicles," *IEEE Trans. Power Electron.*, vol. 28, no. 5, pp. 2151–2169, May. 2013.

[17] N. Wong and M. Kazerani, "A review of bidirectional on-board charger topologies for plugin vehicles," in *Proc. Can. Conf. Elect. Comput. Eng.*, 2012, pp. 1–6.

[18] Y. Du, S. Lukic, B. Jacobson, and A. Huang, "Review of high power isolated bi-directional DC-DC converters for PHEV/EV DC charging infrastructure," in *Proc. IEEE Energy Conversion Congr. Expo.*, Sep. 2011, pp. 553–560.

[19] R. J. Ferreira, L. M. Miranda, R. E. Araujo, and J. P. Lopes, "A new bidirectional charger for vehicle-to-grid integration," in *Proc. IEEE PES Int. Conf. Exhib. Innovative Smart Grid Technol.*, 2011, pp. 1–5.

[20] T. Ngo, K. Lee, J. Won, and K. Nam, "Study of single-phase bidirectional battery charger for high power application," in *Proc. IEEE Power Electron., Motion Contr. Conf.*, 2012, pp. 958–962.

[21] D. Segaran, D. Holmes, and B. P. McGrath, "High-performance bidirectional AC–DC converters for PHEV with minimised DC bus capacitance," in *Proc. IEEE 37th Annu. Conf. Ind. Electron. Soc.*, Nov. 2011, pp. 3620–3625.

[22] M. Rosekeit, C. Broeck, and R. W. De Doncker, "Dynamic control of a dual active bridge for bidirectional ac charging," in *Proc. IEEE Inter. conf. Ind. Tech.*, 2015, pp. 2085–2091.

[23] L. Xue, Z. Shen, D. Boroyevich, P. Mattavelli, and D. Diaz, "Dual active bridge-based battery charger for plug-in hybrid electric vehicle with charging current containing low frequency ripple," *IEEE Trans. Power Electron.*, vol. 30, no. 12, pp. 7299–7307, Dec. 2015.

[24] J. Choi, B. Byen, Y. Lee, D. Han, H. Kho, and G. Choe, "Design of leakage inductance in resonant dc-dc converter for electric vehicle charger," *IEEE Trans. Magnetics*, vol. 48, no. 11, pp. 4417–4420, Nov. 2012.

[25] J. Shin, J. Y. Lee, "An electrolytic capacitor-less bi-directional EV on-board charger using harmonic modulation technique," *IEEE Trans. Power Electron.*, vol. 29, no. 10, pp. 5195–5203, Oct. 2014.

[26] H. Kim, M. Ryu, J. Baek, and J. Jung, "High-efficiency isolated bidirectional ac–dc converter for a dc distribution system," *IEEE Trans. Power Electron.*, vol. 28, no. 4, pp. 1642–1654, Apr. 2013.

[27] M. Ibanez, J. M. Echeverria, J. Vadillo, and L. Fontan, "A step-up bidirectional series resonant dc/dc converter using a continuous current mode," *IEEE Trans. Power Electron.*, vol. 30, no. 3, pp. 1393–1402, Mar. 2015.

[28] Z. U. Zahid, Z. M. Dalala, R. Chen, B. Chen, and J. S. Lai, "Design of bidirectional dc–dc resonant converter for vehicle-to-grid (V2G) applications," *IEEE Trans. Transportation. Electrification*, vol. 1, no. 3, pp. 232–244, Oct. 2015.

[29] T. Jiang, J. Zhang, X. Wu, K. Sheng, and Y. Wang, "A bidirectional LLC resonant converter with automatic forward and backward mode transition," *IEEE Trans. Power Electron.*, vol. 30, no. 2, pp. 757–770, Feb. 2015.

[30] N. Mohan, T. M. Undeland, and W. P. Robbins, *Power Electronics: Converters, Applications, and Design*, 3rd ed. Hoboken, NJ, USA: Wiley, 2003.

[31] T. Shimizu, Y. Jin, and G. Kimura, "DC ripple current reduction on a single-phase PWM voltage-source rectifier," *IEEE Trans. Ind. Appl.*, vol. 36, no. 5, pp. 1419–1429, Sep./Oct. 2000.

[32] S. G. Li, B. Ozpineci, and L. M. Tolbert, "Evaluation of a current source active power filter to reduce the DC bus capacitor in a hybrid electric vehicle traction drive," in *Proc. IEEE Energy Convers. Congr. Expo.*, 2009, pp. 1185–1190.

[33] R. X. Wang, F. Wang, D. Boroyevich, R. Burgos, R. X. Lai, P. Q. Ning, and K. Rajashekara, "A high power density single-phase PWM rectifier with active ripple energy storage," *IEEE Trans. Power Electron.*, vol. 26, no. 5, pp. 1430–1443, May 2011.

[34] H. Wang, H. S. Chung, and W. Liu, "Use of a series voltage compensator for reduction of the dc-link capacitance in a capacitor-supported system," *IEEE Trans. Power Electron.*, vol. 29, no. 3, pp. 1163–1175, Mar 2014.

[35] S. Bala, T. Tengner, P. Rosenfeld, and F. Delince, "The effect of low frequency current ripple on the performance of a Lithium Iron Phosphate (LFP) battery energy storage system," *in Proc. IEEE ECCE*, Sep. 2012, pp. 3485-3492.

[36] T. Kim, J. Jeong, B. Lee, D. Shin, H. Song, B. Kim, and H. Kim, "Analytical study on low-frequency ripple effect of battery charging," *in Proc. Veh. Power Propulsion Conf.*, Oct. 2012, pp. 809–811.

[37] H. Z. Beh, G. A. Covic, and J. T. Boys, "Effects of pulse and DC charging on lithium iron phosphate (LiFePO4) batteries," *in Proc. IEEE Energy Convers. Congr. Expo.*, Sep. 2013, pp. 315–320.

[38] R. Prasad, C. Namuduri, and P. Kollmeyer, "Onboard unidirectional automotive G2V battery charger using sine charging and its effect on li-ion batteries," *in Proc. IEEE Energy Convers. Congr. Expo.*, Sep. 2015, pp. 6299–6305.

[39] R. L. Steigerwald, "A comparison of half-bridge resonant converter topologies," *IEEE Trans. Power Electron.*, vol. 3, no. 2, pp. 174–182, Apr. 1988.

[40] J. Park, M. Kim, S. Choi, "Zero-current switching series loaded resonant converter insensitive to resonant component tolerance for battery charger," *IET Power Electron.*, vol. 7, no. 10, pp. 2517–2524, Dec. 2014.

[41] J. Park, and S. Choi "Design and control of a bidirectional resonant dc–dc converter for automotive engine/battery hybrid power generators," *IEEE Trans. Power Electron.*, vol. 29, no. 7, pp. 3748–3757, Jul. 2014.

[42] S. Yoon, H. Oh, and S. Choi, "Controller design and implementation of indirect current control based utility-interactive inverter system," *IEEE Trans. Power Electron.*, vol. 28, no. 1, pp. 26–30, Jan. 2013.